Recrystallization boundary migration in the 3D heterogeneous microstructure near a hardness indent

Hong, Chuanshi; Zhang, Yubin; Lindkvist, Adam; Liu, Wenjun; Tischler, Jon; Xu, Ruqing; Juul Jensen, Dorte

Published in:
Scripta Materialia

Link to article, DOI:
10.1016/j.scriptamat.2021.114187

Publication date:
2021

Document Version
Publisher's PDF, also known as Version of record

Scripta Materialia 205 (2021) 114187

Contents lists available at ScienceDirect

Scripta Materialia

journal homepage: www.elsevier.com/locate/scriptamat

Recrystallization boundary migration in the 3D heterogeneous microstructure near a hardness indent

Chuanshi Hong[a,*], Yubin Zhang[a], Adam Lindkvist[a], Wenjun Liu[b], Jon Tischler[b], Ruqing Xu[b], Dorte Juul Jensen[b,*]

[a] Department of Mechanical Engineering, Technical University of Denmark, DK-2800 Kgs Lyngby, Denmark
[b] Advanced Photon Source, Argonne National Laboratory, Argonne, Illinois, 60439, USA

ARTICLE INFO

Article history:
Received 19 April 2021
Revised 1 July 2021
Accepted 30 July 2021

Keywords:
Recrystallization
Grain boundary migration
Synchrotron radiation
3D reconstruction
Heterostructures

ABSTRACT

Boundary migration during recrystallization in the heterogeneous microstructure near a hardness indent in lightly rolled pure Al was followed in 3D. The microstructure after multiple steps of ex-situ annealing was examined using synchrotron white-beam differential-aperture X-ray microscopy, supplemented by scanning electron microscopy. Heterogeneous recrystallization boundary migration was observed and analyzed in terms of driving force and boundary characteristics. The results reveal very similar local stored energies and boundary misorientations for the migrating and stationary boundary segments, whereas the grain boundary normals differ significantly. Effects of grain boundary mobility and deformation microstructure morphology on the migration are discussed.

Hetero-structural metals is a hot topic in materials science [1,2]. This class of materials includes gradient and layered structured metals, i.e. metals with microstructural variations on a rather large scale. Heterogeneous microstructures are however also present on finer scales (e.g. [3]): It is well documented that for metals deforming by slip, the deformation microstructure depends on the grain orientation [4]. There will thus be grain to grain variations within the deformation microstructure. Additionally, even within a grain, the microstructure is heterogeneous; for example geometrically necessary boundaries with relatively high misorientation exist in a matrix of cells with lower misorientation across the cell boundaries and almost no dislocations inside the cells [5–7].

All these “within grain” and “grain to grain” variations affect the properties and are important for the microstructural evolution during subsequent processing and use. The importance of fine-scale heterogeneities has so far been much less recognized than coarse scale ones.

The present work focuses on effects of “within grain” variations on boundary migration during recrystallization. It is well known that the main driving force for recrystallization is the energy stored in the deformed matrix [8]. When the deformation microstructure is heterogeneous, so is the local distribution of stored energy. Effects of such heterogeneities on the boundary migration during recrystallization has only recently been considered [9–11] and it has been suggested that besides the *local* stored energy distribution also the deformation microstructure morphology is of key importance [11,12].

The aim of this work is to investigate how a recrystallization boundary migrates through the deformation microstructure near a hardness indent in lightly rolled aluminum. This system is chosen so that the hardness indent can stimulate nucleation [12], and the light rolling together with the hardness indent result in a rather complex deformation microstructure [13,14] that still can be precisely mapped in 3D. Compared to previous work on this topic [9–11,15], the present investigation is unique, because i) it is in full 4D (x, y, z, time), so complete information about the matrix and the growing grain is available, and ii) the deformation microstructure and the orientation relationship between growing grain and matrix are different from those in the only other 4D investigation [15]. The latter is important to test the hypothesis that: the deformation microstructure morphology, not only the stored energy distribution, is important for boundary migration.

For the present investigation we have used white-beam differential-aperture X-ray microscopy (DAXM) available at 34-ID-E at the Advanced Photon Source (APS), Argonne National Laboratory, USA [16]. This method allows complete non-destructive 3D mapping of the deformation microstructure with a crystallographic orientation resolution of about 0.01° [17,18]. Also the nuclei formed at hardness indents can be imaged [12] and their growth may be monitored after ex-situ annealing (i.e. mapping

* Corresponding authors.
E-mail addresses: cshong@imr.ac.cn (C. Hong), doje@mek.dtu.dk (D. Juul Jensen).

https://doi.org/10.1016/j.scriptamat.2021.114187

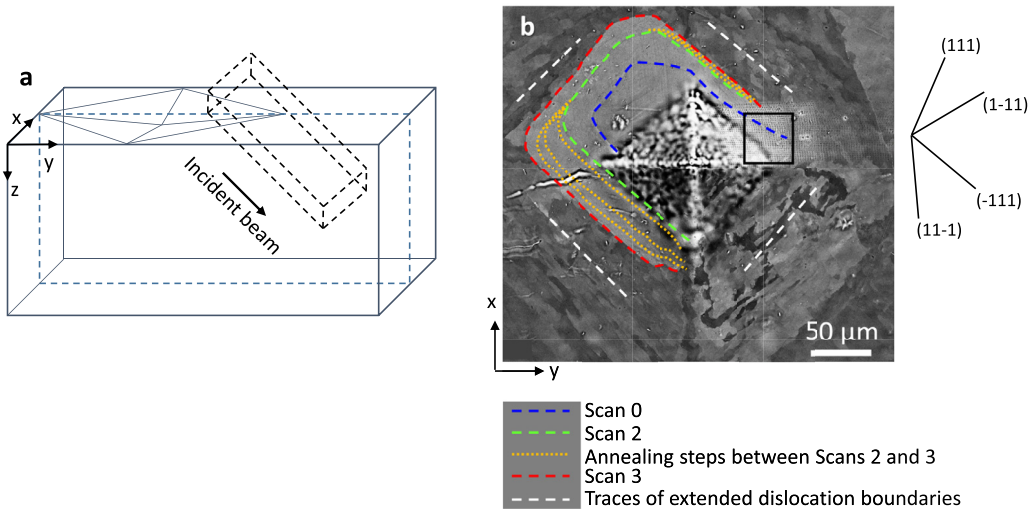

Fig. 1. (a) A schematic illustration of the relative position of the sample, the micro hardness indent and the scanned volume by DAXM. Crystallographic orientations are based on the sample coordinate system with basis vectors x, y and z, which correspond to the normal, rolling and transverse directions of the rolling geometry. The dashed cuboid indicates the volume scanned by DAXM. The incident beam, marked by an arrow, lies in the y-z plane and is inclined at 45° to the y direction. (b) SEM-ECC micrograph showing the indent and the recrystallized grain, Grain-R, on the x-y plane corresponding to Scan 3. The coloured dashed/dotted lines mark the positions of the boundary at various stage of annealing as described below the figure. Note that the sample at the state of Scan 1 was not examined by SEM-ECC due to limited access to microscopes at the synchrotron facility. The white dashed lines approximately mark the traces of dislocation boundaries in the four quadrants of the indent. The solid lines to the right of the figure indicate the intersections between the x-y plane and the {1 1 1} planes of Grain-R. The rectangle marks the region illuminated by the X-ray beam during DAXM.

the same nucleus/grain after a number of annealing steps in a furnace outside the microscope).

Such data allows a complete analysis of how a migrating recrystallization boundary interacts with the deformation induced boundaries in a complex hetero-structured matrix.

The investigated Al plate has a purity of 99.996 wt.% and was 94 × 46 × 3 mm^3 in size. The plate was fully annealed at 600 °C for 7 days, resulting in grain sizes on the millimeter scale, and subsequently rolled at room temperature to a thickness reduction of 12% (true stain of 0.128). From this plate, thin slices of ~15 × 1 × 3 mm^3 were cut parallel to the longitudinal section (containing the normal (ND) and the rolling (RD) direction), using a diamond saw. The slices were mechanically ground and polished on both sectioning surfaces, followed by electro-chemical polishing.

Vickers hardness indents were made on one sectioning surface of a few slices containing parts of the same original grain, to stimulate nucleation. To obtain an initial recrystallized grain with a size of ~100 μm, ideal for DAXM, a series of annealing experiments with different combinations of indentation load and annealing temperature were first carried out. By annealing at 335°C for 10 min, a recrystallized grain was selected which had formed at a 1 kg load indentation (Fig. S1 in Supplementary materials and Fig. 1). The recrystallized grain is located near the bottom of the indent, and therefore the indented side of this slice was further ground to remove about half the depth of the indent, followed by electro-chemical polishing to facilitate DAXM measurements. A volume, containing the recrystallized grain, is then characterized by DAXM, which is referred to as Scan 0. Afterwards, without further polishing, the slice received three sets of additional annealing treatments to achieve significant growth of the recrystallizing grain. 3D scans were made after each of the annealing treatments, and are referred to as Scans 1, 2 and 3, respectively (Fig. S1).

For the DAXM measurements, the focused polychromatic X-ray microbeam had a full-width half maximum of ~0.3 μm, and the scans were performed with a step size of 1.5 μm which is thus the voxel size of the present 3D reconstruction. The 3D data is processed and visualized using Dream3D and Paraview. Quantification of grain boundary characteristics and stored energies was carried out using in-house developed Matlab codes and the open-source toolbox, MTEX [19].

Fig. 1 shows the geometry of the DAXM experiment. The incident X-ray microbeam penetrates the sample at an angle of 45°. A volume of 39 × 130.5 × 42 μm^3, as outlined by the dashed cuboid in Fig. 1a, is characterized in each of the four 3D scans. As measured from DAXM, the mean orientation of the recrystallized grain is determined by x = [0.822 -0.578 0.114] and y = [0.196 0.089 -0.977], corresponding to Bunge Euler angles of (6.7°, 79.5°, 32.9°), where x and y is ND and RD of the rolling geometry, respectively. The mean orientation of the deformed grain in the region far from the indent has x = [0.928 -0.349 0.129] and y = [0.067 -0.186 -0.980], corresponding to Bunge Euler angles of (7.5°, 98.6°, 21.7°). Compared to the region far from the indent, the indented region has rotated by up to 11°.

Morphologically, the deformed microstructure in the indentation-affected region can be divided into four quadrants as defined by the diagonal lines of the indent, as observed by SEM-ECC (Fig. 1b). Elongated dislocation cell structures have been developed in each quadrant and have an average boundary spacing of ~1.2 μm in their short-axis directions. The cell structures are oriented differently in each quadrant in a way that their longer axes are roughly parallel to the edge of the indent in that quadrant. This microstructure is different from that in the rolled matrix far away from the indent, where a cell-block dislocation structure typical of rolling deformation [5–7] has been observed and has a larger short-axis average boundary spacing of ~6.1 μm. These observations indicate that the microstructure near the indent is dominated by indentation rather than rolling, which is reasonable since the maximum indentation strain (in the range: 0.25 to 0.36 [20]) is significantly larger compared with the rolling true strain (0.128).

The growth of the recrystallized grain (hereafter referred to as Grain-R) subjected to annealing can be seen in 2D from SEM-ECC observations (Fig. 1b). The growth is heterogeneous: Grain-R grows in all indent quadrants except the lower right one. The migrating boundary segments show a strong tendency to remain relatively straight and roughly parallel to the indent edge (*and the traces of the extended/planar dislocation boundaries*). The relatively straight

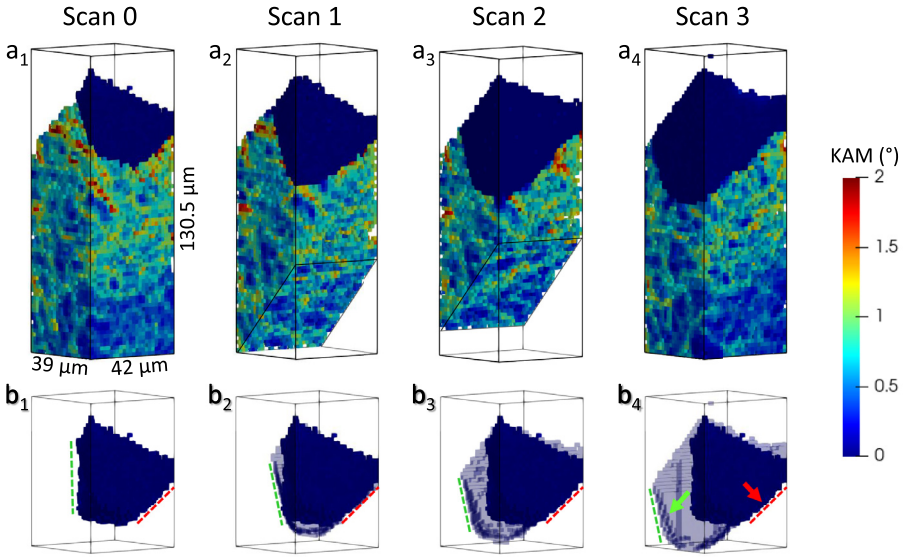

Fig. 2. (a_1–a_4) DAXM reconstruction coloured using Kernel average misorientation (KAM). The bottom parts of the volume in Scans 1 and 2 are not covered by the DAXM. (b_1–b_4) Evolution of Grain-R. The original shape of Grain-R (Scan 0) is shown in full opacity in all scans as a reference, while the new volumes in Scans 1 to 3 are shown in 20% opacity. The green dashed lines and arrow in b_4 indicates the migrating flat boundary segment and the red ones indicate the non-migrating flat segment.

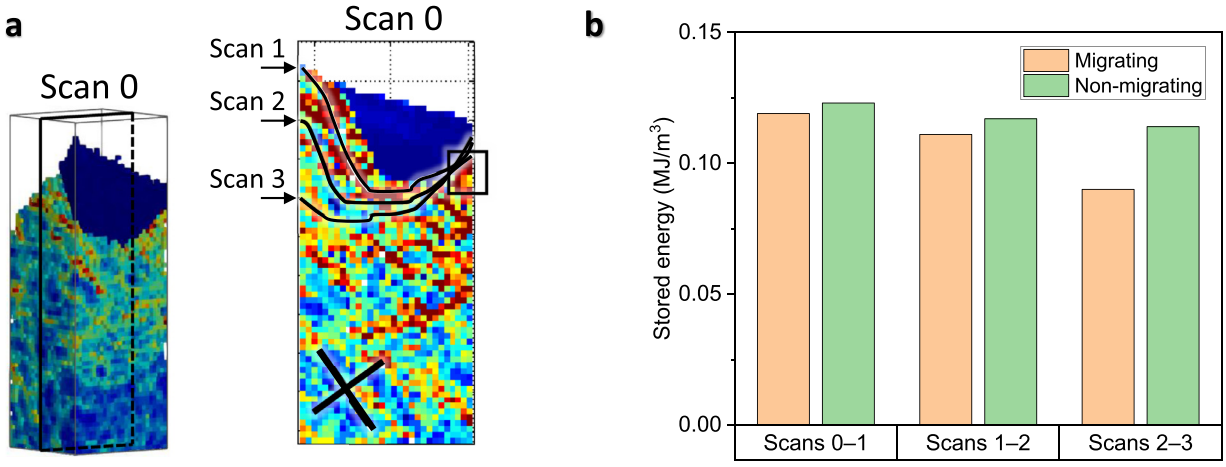

Fig. 3. Relation between the stored energy and boundary migration. (a) The volumes consumed by boundary migration. The left-hand figure shows a section in the DAXM reconstruction of Scan 0, of which a KAM map is shown in the right-hand figure. In the right-hand figure the black curves indicate the positions of the boundary in Scans 1, 2 and 3. (Note that the seemingly planar parts near the bottom of the grain boundary in Scan 2 and Scan 3 are a misimpression when showing 3D information in 2D sections.) The rectangle marks where the stored energy was calculated for the non-migrating segment. The two solid black lines indicate tendency of elongated dislocation structures. (b) Stored energies.

boundary segments on the upper-right and lower-left sides coincide with the traces of (-1 1 1) planes of both Grain-R and the deformed grain, while the upper-left boundary segment does not appear to coincide with any of the {1 1 1}, {1 1 0} or {1 0 0} plane traces of either grain.

The DAXM mapped 3D region contains both migrating and non-migrating boundary segments surrounding Grain-R. The evolution of the microstructure through the four scans are shown in Fig. 2 (See also Fig. S2 in Supplementary materials). The boundary of Grain-R is viewed nearly edge-on. The figure reveals that while the morphology of the dislocation structure in the matrix remains largely unchanged, Grain-R grows considerably and heterogeneously in 3D. Grain-R grows from Scan 0 to Scan 3 in the lower left direction (i.e. into the upper right quadrant in Fig. 1b), but remains stationary in its lower right direction (i.e. towards the lower right quadrant in Fig. 1b), as indicated by arrows in Fig. 2b_4. The boundary between Grain-R and the deformed grain consists of three parts: i) a relatively flat, migrating segment marked by green dashed lines, ii) a relatively flat, non-migrating segment marked by red dashed lines, and iii) a curved transitional part connecting the two flat segments.

The driving force for boundary migration arises from the stored energy within the deformed microstructure [8] and the surface energy associated with curvature of the boundary [9]. In the present case, both the migrating and the non-migrating segments are remarkably flat; any curvature-related surface energy can thus be neglected here. In pure metals (as the present), the boundary mobility is mainly related with the angle and axis of misorientation across the boundary and with the boundary plane. The migration of the boundary surrounding Grain-R is therefore analyzed in terms of stored energy, boundary misorientation and boundary plane in the following.

The stored energy in front of Grain-R was calculated based on the misorientation angles across the dislocation boundaries in the deformed grain according to the Read-Shockley equation, as described in [15,21] (See Supplemental Materials for details). This calculation is accounting for most of the stored energy in particular for Al where dynamic recovery has reduced the number of loose

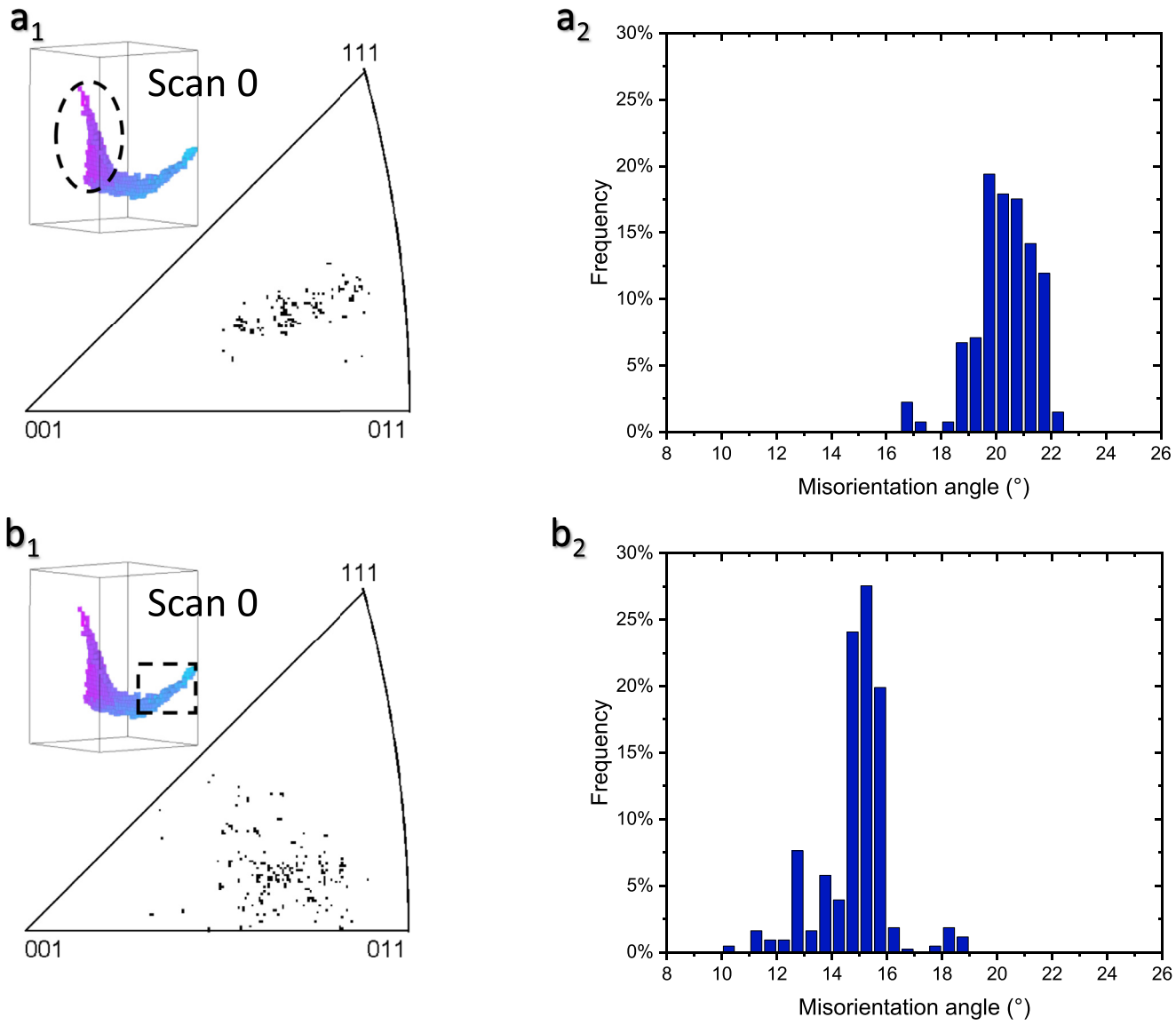

Fig. 4. Relation between boundary misorientation and boundary migration. (a_1 & a_2) The distribution of boundary misorientation axes in an inverse pole figure (a_1) and histogram distribution of boundary misorientation angles (a_2) of the migrating flat segment of the boundary. (b_1 & b_2) Analysis of the non-migrating flat segment of the boundary in the same way as (a_1 & a_2). The insets show the grain boundary, where migrating flat segment and the non-migrating flat segment are outlined.

dislocations. As sketched in Fig. 3a, for the migrating segment, the volume consumed by Grain-R between every two neighboring 3D scans was used for such calculations. For the non-migrating segment, the volume within a few micrometers from the boundary of Grain-R was used. The average stored energies in the volumes consumed in the intervals Scans 0–1, Scans 1–2 and Scans 2–3 are 0.119, 0.111 and 0.090 MJ/m^3, respectively, whereas the average stored energies in front of the non-moving segment are 0.123, 0.117 and 0.114 MJ/m^3 (Fig. 3b). Notice that the stored energies decrease from Scans 0–1 to Scans 2–3, which agrees with the expectation of some recovery in the deformed structure during annealing. The stored energy in front of the migrating boundary decreases more than that in front of the non-migrating part. This is attributed to the gradient in the stored energy: as the boundary migrates into deeper regions beneath the indented surface, the stored energy decreases from the high level given by the indentation to the lower level of the rolling. The results show no advantage for the migrating boundary segment in terms of stored energy compared with the non-migrating segment.

The step size of an orientation scan is known to influence the calculated stored energy. To obtain a reliable value, the step size should be on the same scale as the microstructural sizes [22], which is fulfilled in the present case; the step size (1.5 μm) is comparable to the smallest mean boundary spacing in the scanned volume (1.2 μm on the indented surface). To test the effects of step size, a calculation skipping every other voxel (i.e. doubling the step size) was carried out. This results in slightly decreased values (21–29%) with roughly the same effect for different regions and does not change the conclusion that stored energy differences cannot explain the observed migration differences (Fig. S3).

The misorientation across the boundary between Grain-R and the deformed matrix in Scan 0 is shown in Fig. 4. The mean directions of the misorientation axes of the migrating and non-migrating flat segments are close, being [-0.571 0.182 0.800] and [-0.529 0.152 0.835], respectively, which are only 3.6° apart. The axes of the non-migrating part scatter more than that of the migrating part and cover a slightly different region in the inverse pole figure. The misorientation angles across the migrating flat segment are on average ~5° larger than that across the non-migrating one. For the migrating parts there are no misorientation angles less than 15°, whereas for the non-migrating parts 47% of the misorientations are less than 15°. Similar results were observed in Scans 1, 2 and

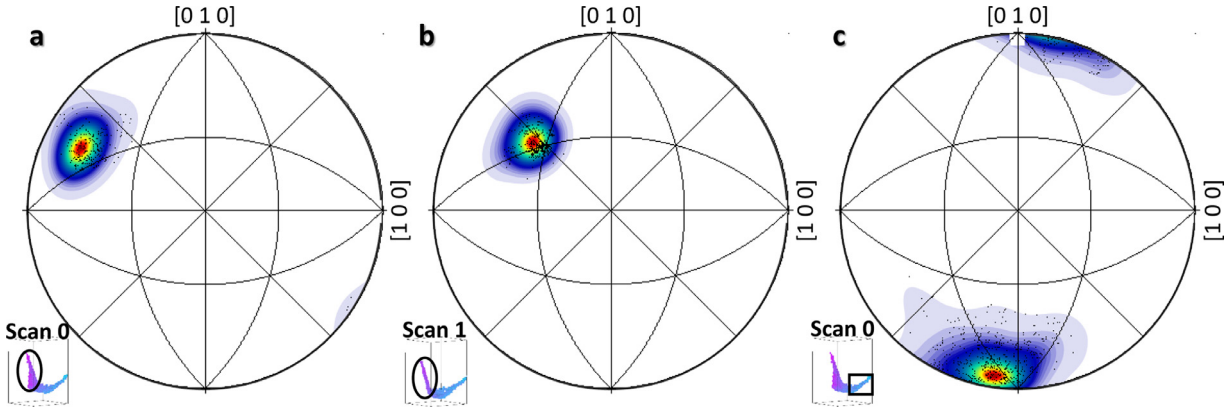

Fig. 5. Relation between boundary plane normal and boundary migration. (a & b) Distribution of the normal direction of the boundary plane for the migrating boundary segment in Scans 0 and 1. (c) Distribution of the normal direction of the non-migrating boundary segment in Scan 0.

3 (Figs. S3 and S4). Even with the limited knowledge we already have regarding the influence of misorientation axis on migration, it could be stated that this small difference is unlikely to be a determining factor, although the migrating segment might have a slight advantage compared to the non-migrating one, because of less orientation pinning [23].

The boundary plane of the migrating flat segment is completely different from that of the non-migrating part (Fig. 5). In Scan 0, the boundary plane normal of the migrating segment scatters around [-0.858 0.424 0.290] (Fig. 5a), which is 24.8° from [-1 1 1]; by contrast, that of the non-migrating segment scatters around [-0.174 -0.981 0.086] (Fig. 5c), which is 11.2° from [0 -1 0]. After subsequent annealing, the boundary plane normal of the migrating flat segment becomes [-0.625 0.568 0.533] in Scan 1 (Fig. 5b), [-0.543 0.598 0.589] in Scan 2 and [-0.444 0.708 0.549] in Scan 3, which are 3.8°, 2.4° and 10.8° from [-1 1 1], respectively. The obvious difference in the grain boundary plane between the migrating and non-migrating segments suggests the grain boundary plane may be a key factor for the migration.

The morphology of the dislocation structure in front of the recrystallizing grain may also affect its growth [10,15]. In the present case, SEM-ECC observation of the sample surface has shown elongated dislocation cell structures (Fig. 1b), which is supplemented by the DAXM results (Fig. 3a), and the migrating recrystallization boundary segments align roughly parallel to this structure.

To clarify the relative importance of grain boundary plane and deformation microstructure morphology on boundary migration, the present results may be used as input for molecular dynamics simulations. Such simulations will reveal if the difference in grain boundary normal can explain the observed migration rate differences or not, and therefore, indirectly show if also the deformation microstructure morphology is of importance.

In conclusion, the heterogeneous migration of the boundary surrounding a recrystallizing grain cannot be accounted for by the differences in local stored energy within the deformed structure. While effects of the misorientation between the recrystallized grain and the deformed structure remains plausible, the relation between the grain boundary plane normal and grain boundary migration is significant. The results underline the importance of a full 4D (x, y, z, time) characterization in particular in resolving grain boundary plane effects which cannot be done otherwise.

Declaration of Competing Interest

The authors declare that they have no known competing financial interests or personal relationships that could have appeared to influence the work reported in this paper.

Acknowledgment

This work was supported by the European Research Council (ERC) under the European Union's Horizon 2020 research and innovation program [grant number 788567]. Use of the Advanced Photon Source was supported by the U. S. Department of Energy, Office of Science, Office of Basic Energy Sciences, under Contract No. DE-AC02- 06CH11357. The authors thank Dr Chaoling Xu for providing the samples in the rolled state.

Supplementary materials

Supplementary material associated with this article can be found, in the online version, at doi:10.1016/j.scriptamat.2021.114187.

Reference

[1] X. Wu, Y. Zhu, Mater. Res. Lett. 5 (2017) 527–532.
[2] Y. Zhu, K. Ameyama, P.M. Anderson, I.J. Beyerlein, H. Gao, H.S. Kim, E. Lavernia, S. Mathaudhu, H. Mughrabi, R.O. Ritchie, N. Tsuji, X. Zhang, X. Wu, Mater. Res. Lett. 9 (2021) 1–31.
[3] D. Juul Jensen, F.X. Lin, Y.B. Zhang, Y.H. Zhang, Mater. Sci. Forum 753 (2013) 37–41.
[4] X. Huang, G. Winther, Philos. Mag. 87 (2007) 5189–5214.
[5] C. Hong, X. Huang, G. Winther, Philos. Mag. 93 (2013) 3118–3141.
[6] A. Godfrey, D. Juul Jensen, N. Hansen, Acta Mater. 46 (1998) 835–848.
[7] W. Pantleon, N. Hansen, Acta Mater 49 (2001) 1479–1493.
[8] F.J. Humphreys, G.S. Rohrer, A.D. Rollett, Recrystallization and Related Annealing Phenomena, Elsevier, 2017.
[9] Y. Zhang, A. Godfrey, D. Juul Jensen, Scr. Mater. 64 (2011) 331–334.
[10] Y. Zhang, A. Godfrey, D. Juul Jensen, Metall. Mater. Trans. A 45 (2014) 2899–2905.
[11] G.H. Fan, Y.B. Zhang, J.H. Driver, D. Juul Jensen, Scr. Mater. 72–73 (2014) 9–12.
[12] C. Xu, Y. Zhang, A. Godfrey, G. Wu, W. Liu, J.Z. Tischler, Q. Liu, D. Juul Jensen, Sci. Rep. 7 (2017) 42508.
[13] M. Rester, C. Motz, R. Pippan, Acta Mater. 55 (2007) 6427–6435.
[14] E. Demir, D. Raabe, N. Zaafarani, S. Zaefferer, Acta Mater. 57 (2009) 559–569.
[15] Y.B. Zhang, J.D. Budai, J.Z. Tischler, W. Liu, R. Xu, E.R. Homer, A. Godfrey, D. Juul Jensen, Sci. Rep. 7 (2017) 4423.
[16] B.C. Larson, W. Yang, G.E. Ice, J.D. Budai, J.Z. Tischler, Nature 415 (2002) 887–890.
[17] Y.F. Gao, B.C. Larson, J.H. Lee, L. Nicola, J.Z. Tischler, G.M. Pharr, Y. Huan, J. Appl. Mech. Trans. ASME 82 (2015) 061007–1–10.
[18] B.C. Larson, L.E. Levine, J. Appl. Crystallogr. 46 (2013) 153–164.
[19] F. Bachmann, R. Hielscher, H. Schaeben, in: Solid State Phenom., 160, Trans Tech Publications Ltd, 2010, pp. 63–68.
[20] M.M. Chaudhri, Acta Mater. 46 (1998) 3047–3056.
[21] A. Godfrey, O.V. Mishin, T. Yu, in: Proc. 36th Risø Int. Symp. Mater. Sci. IOP Conf. Ser. Mater. Sci. Eng., IOP Publishing, 2015.
[22] D.P. Field, C.C. Merriman, N. Allain-Bonasso, F. Wagner, Model. Simul. Mater. Sci. Eng. 20 (2012) 024007.
[23] D. Juul Jensen, Acta Metall. Mater. 43 (1995) 4117–4129.